EPR Spectroscopy of Some Mn^{2+} Doped Langbeinites with Regard to Low Temperature Phases

T. Böttjer and M. Stockhausen

Institut für Physikalische Chemie der Universität Münster, D-48149 Münster (Germany)

Z. Naturforsch. **51a**, 1084–1090 (1996); received June 16, 1996

Electron paramagnetic resonance (EPR) spectra of Mn^{2+} centers in 11 langbeinites, $A_2^+B_2^{2+}(SO_4)_3^{2-}$, with $A^+ = NH_4^+, K^+, Rb^+$ or Tl^+ and $B^{2+} = Mg^{2+}, Ca^{2+}, Zn^{2+}$ or Cd^{2+}, are measured over relatively large temperature ranges chosen to cover phase transitions, if any. For 7 langbeinites which do not contain Mg^{2+}, phase transitions are observed, but no more than one low temperature phase is distinguishable by EPR. Except for the K–Zn langbeinite, only one defect center is noticeable in that phase. The low temperature EPR parameters are reported, and their temperature dependence is discussed with respect to correlations between structure and phase transition characteristics and to the trigger mechanism.

Introduction

Sulfates of the $A_2^+B_2^{2+}(SO_4)_3^{2-}$ type, commonly termed langbeinites, are known with $A^+ = NH_4^+, K^+$, Rb^+, Cs^+ or Tl^+, and $B^{2+} = Mg^{2+}$, Ca^{2+}, Mn^{2+}, Fe^{2+}, Co^{2+}, Ni^{2+}, Zn^{2+} or Cd^{2+} [1–3]. At sufficiently high temperature, they crystallize isomorphously in the cubic space group $P2_13$, the unit cell containing two non-equivalent sites for both the monovalent A and the divalent B cations along the threefold [111] axis [1, 2, 4–7].

On decreasing temperature, phase transitions have been observed for several langbeinites by various experimental methods. It was inferred that they lead to space groups of lower symmetry, namely monoclinic ($P2_1$), triclinic (P1) or orthorhombic ($P2_12_12_1$) [2, 6, 8–12]. Structure determinations which substantiate those assignments are available for langbeinites in the orthorhombic phase $P2_12_12_1$ [2, 6, 13–15]. They show that the phase transition is connected with a minor displacement of atoms from the sites occupied in the high temperature phase $P2_13$. Also the structural differences between $P2_13$ and $P2_1$ as well as P1 appear to be small [16].

The available data were combined by Hikita et al. [17] to a tentative classification of langbeinites according to the succession of phases on decreasing temperature. The first class shows transitions $P2_13 \rightarrow P2_1 \rightarrow P1 \rightarrow P2_12_12_1$, the second one $P2_13 \rightarrow P2_12_12_1$. The third class shows no phase transitions at all.

While the cubic high temperature phase is parelectric [8, 11, 18], low temperature phases were found to be ferroelectric ($P2_1$, P1) [8, 18–20] and ferroelastic ($P2_12_12_1$) [8, 13, 18, 21]. The term "improper ferroelectricity" is used since the phase transition is *not* triggered by spontaneous polarization [22]. The trigger mechanism is not yet well understood.

A suitable method to gather information on the different phases and on the transition mechanisms is electron paramagnetic resonance (EPR) of langbeinites which are doped with paramagnetic ions, since EPR probes the local structure and the point symmetry of the ion's immediate environment. In particular Mn^{2+} has been employed for that purpose [23–29]. EPR studies of the high temperature phase of langbeinites have shown that Mn^{2+} is substitutionally incorporated into both B^{2+} sites, prefering the more spacious one. The temperature dependence of EPR parameters has been studied with langbeinites of type NH_4–Cd [25, 26], Rb–Cd [27, 29] and Tl–Cd [28]. Approaching the phase transition from the high temperature side, a decrease of the zero field splitting (ZFS) parameter $|B_2^0|$ and an increae of linewidths was observed. Furthermore, an increase of hyperfine splitting was found in case of the NH_4–Cd langbeinite.

In continuation of our previous EPR work on the high temperature phase of Mn^{2+} doped langbeinites [23], the present communication deals with the temperature dependence of the EPR parameters, looking at structural information about low temperature phases and, eventually, about precursor effects. Even qualitative EPR data are hoped to aid the interpretation of phase transition mechanisms. A re-examina-

Reprint requests to Prof. M. Stockhausen.

0932-0784 / 96 / 1000-1084 $ 06.00 © – Verlag der Zeitschrift für Naturforschung, D-72072 Tübingen

Table 1. Manganese doped langbeinites as studied in this work, and literature data on their phase transitions.

Langbeinite		Range	LT[b]	Samples		Transition temp. T_P/K[d] to				Ref.[e]
A	B	of T[a]		SC	P	$P2_1$	P1	P?	$P2_12_12_1$	
NH_4	Mg	I			×	–	–	–	221	[33]
						–	–	241	220	[3]
K	Mg	I		×		63.8	54.9	–	51.0	[34, 35], [2]
Rb	Mg	I		×		–	–	–	–	[35]
Tl	Mg	I			×	–	–	230.8	227.8	[3]
K	Ca	II	×		×	–	–	–	457*	[2]
Rb	Ca	I, II	×		×	183*	–	–	–	[33]
K	Zn	I	×	×	×	138(*)	–	–	–	[2], [35]
						137	–	87	–	[17], [36]
NH_4	Cd	I	×	×		95*	–	–	–	[37], [38]
						94.5	–	–	–	[26]
						93	–	–	–	[3]
						92	–	–	–	[32], [39]
K	Cd	II	×	×		–	–	–	432*	[2], [5, 13, 21, 24]
						–	–	–	431	[40], [35, 38]
						–	–	–	430	[41], [31, 35, 42]
Rb	Cd	I	×	×	×	129(*)	103	–	68	[9, 19], [17, 20, 30]
						129	102	–	–	[29], [27]
						129	97	–	64.5	[3], [16]
Tl	Cd	I	×	×		130.5	121.0	–	94.5*	[28], [18]
						130	127	–	98	[8]
						129	121	–	96.7	[30], [17]
						128	120	–	92	[32], [18]
						127.5	121	107	95.5	[3]

[a] Temperature range studied: I $\approx 50 \cdots 300$ K; II $\approx 300 \cdots 600$ K. – [b] Low temperature phase found and measured. – [c] SC: Single crystal measurements; P: Powder measurements. – [d] T_P denotes the temperature of transition to the symmetry quoted as occuring on decreasing temperature. If there is uncertainty concerning the symmetries involved, the assignment of space groups is only tentatively concluded from the Hikita classification [17]. – [e] The reference from which T_P is taken is quoted separately in the first place. – * T_P value evidenced in the present work as phase transition.

tion of transition temperatures already known from the literature is not intended.

Experimental

The Mn^{2+} doped langbeinites recorded in Table 1 were synthesized from the melt or from aqueous solution as described elsewhere [23]. The table gives also their phase transition temperatures as found in the literature.

EPR spectra at different temperatures were measured with either single crystals or powders (Tab. 1). In the case of single crystals of langbeinites which at room temperature belong to the cubic space group, the threefold axis was oriented parallel to the external magnetic field.

Spectra were obtained at X-band by use of Bruker ESP300 and (sometimes) BER414 spectrometers. Temperatures ranging between about 50 K and 600 K were controlled by either a closed cycle system (low temperatures) or a gas flux system (high temperatures). Although temperatures were well reproducible, their absolute values were uncertain in the order of ± 10 K. A langbeinite with well known transition temperature was used as reference, namely NH_4–Cd (Table 1), the phase transition of which is clearly discernible by EPR [26]. This material responded immediately and reversibly to small changes of temperature (a hysteresis as reported elsewhere [3] was not observed). Crystals containing different amounts of dopant $\lesssim 3$ mole percent did not show any significant influence on the phase transition temperature up to that concentration. The Mn^{2+} concentration of all the other substances studied was $\lesssim 1$ mole percent.

Analysis of EPR Spectra

EPR parameters were obtained according to the spin-Hamiltonian $\mathcal{H} = \mathcal{H}_Z + \mathcal{H}_{ZFS} + \mathcal{H}_{HFS}$ with

$$\mathcal{H}_Z = \beta \boldsymbol{B}_0 \hat{g} \boldsymbol{S}, \quad \mathcal{H}_{ZFS} = \sum_{n=2,\text{even}}^{2\cdot S} \sum_{m=-n}^{n} B_n^m \mathcal{O}_n^m,$$

$$\mathcal{H}_{HFS} = \boldsymbol{S} \hat{A} \boldsymbol{I},$$

viz. using the spherical operator representation for the zero field splitting term $\mathcal{H}_{ZFS}$. Fitting and simulation techniques for parameter determination, in particular from powder spectra, have been described previously [23]. Within experimental uncertainty the g-factor could be assigned an isotropic value $g = 2.0023$ in all cases. It was sufficient to take into account only the sextet centers, viz. to include only the second order ZFS parameters B_2^0 and B_2^2 in the fitting procedure, while the hyperfine structure (HFS) parameters A_i ($i = x, y, z$) could be taken directly from the spectra by averaging over all transitions assigned to the respective direction. It is difficult to obtain A_x and A_y from powder spectra, so these values are more uncertain than A_z and have been even inaccessible in some cases.

Results

EPR spectra were measured for the langbeinites listed in Table 1 in about 10 K steps over the temperature ranges given in the table, which include the phase transition, if any. No EPR detectable phase transition was found with the four Mg langbeinites, except perhaps for K–Mg where a transition around 64 K [34] cannot be excluded from our spectra.

For the other seven langbeinites studied, phase transitions could be observed as alteration of EPR spectral features (in comparison to those of the cubic phase) which occured in some cases within a rather small temperature range (K–Ca, NH_4–Cd, K–Cd, Tl–Cd), in others as continuous variation over a larger temperature range (Rb–Ca, K–Zn, Rb–Cd). An example is illustrated in Fig. 1 which shows peak positions as function of temperature. Phase transitions are also recognizable as discontinuity of the EPR parameters B_2^m (magnitude and sign) and A_i. It should be mentioned as a noteworthy feature that the parameter B_2^2 is negligible for the cubic phase but is necessary for the low-temperature phases. The transition temperatures T_P detected by EPR are, within experimental uncertainty, in accordance with the literature values marked by an asterisk in Table 1.

No more than one phase transition could unambiguously be gathered from the EPR spectra. In cases where several transitions have been observed by other experimental methods (Rb–Cd, Tl–Cd), the different low temperature phases are obviously indistinguishable by EPR.

In the following we report first the EPR parameters of the low temperature phases for appropriately chosen fixed temperatures and describe subsequently their variation with temperature.

EPR Parameters of Low Temperature Phases

The results regarded in this section were obtained at temperatures sufficiently below both the phase transition detectable by EPR and the lowest transition temperature known from the literature. As an example, Fig. 2 shows the experimental and simulated powder spectrum of K–Ca langbeinite in its low temperature phase, which in that case is known from X-ray structure determination to obey $P2_12_12_1$ symmetry. The spectrum reveals the characteristics of triclinic Mn^{2+} centers. Zero field splitting exceeds markedly that of axial centers, and the large number of peaks in the low and high field range which are due to x, y transitions is indicative of a significant rhombic splitting parameter B_2^2.

The EPR parameters of all langbeinites studied in their low temperature phases are collected in Table 2.

Table 2. EPR parameters of the low temperature phase of langbeinites.

Langbeinite		T	Phase	B_2^0	B_2^2	$-A_x$	$-A_y$	$-A_z$	$\frac{A_z(\text{low})}{A_z(\text{high})}$
A	B	(K)		(GHz)	(GHz)		(MHz)		
K	Ca	RT	$P2_12_12_1$	+0.313(3)	+0.127(6)	267(5)	273(5)	273(5)	0.84(2)
Rb	Ca	159	$P2_1$	−0.317(8)	−0.023(2)	285(8)	295(8)	283(8)	1.11(3)
K	Zn(1)[a]	52	$P2_1$	∓0.44(1)	∓0.035(5)	283(8)	285(8)	273(8)	
K	Zn(2)[a]	52	$P2_1$	−0.29(1)	−0.057(5)		275(8)	283(5)	1.16(9)
NH_4	Cd	48	$P2_1$	(−)0.289(3)	(−)0.036(7)		285(8)	287(8)	1.01(2)
K	Cd	RT	$P2_12_12_1$	+0.374(1)	+0.056(5)	275(5)	275(8)	270(5)	0.90(2)
Rb	Cd	52	$P2_12_12_1$?	±0.47(1)	±0.07(2)		275(8)	290(8)	
Tl	Cd	52	$P2_12_12_1$	(+)0.313(5)	(+)0.009(8)		280(8)	293(8)	0.93(4)

[a] For K–Zn langbeinite, the fit suggested two centers.

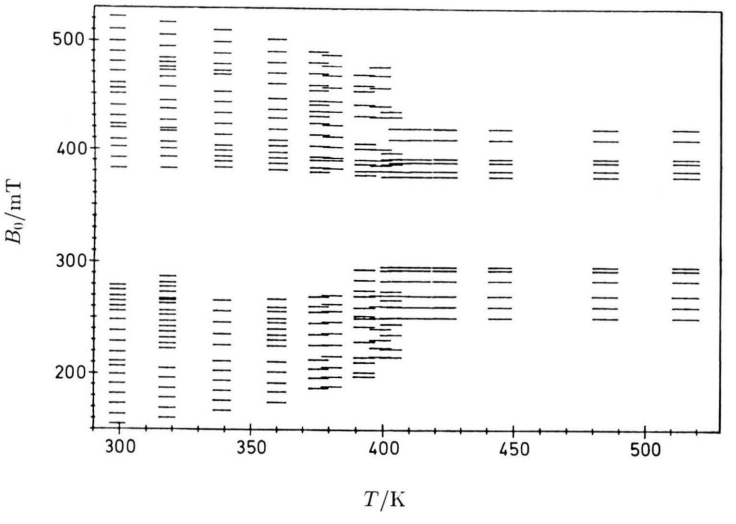

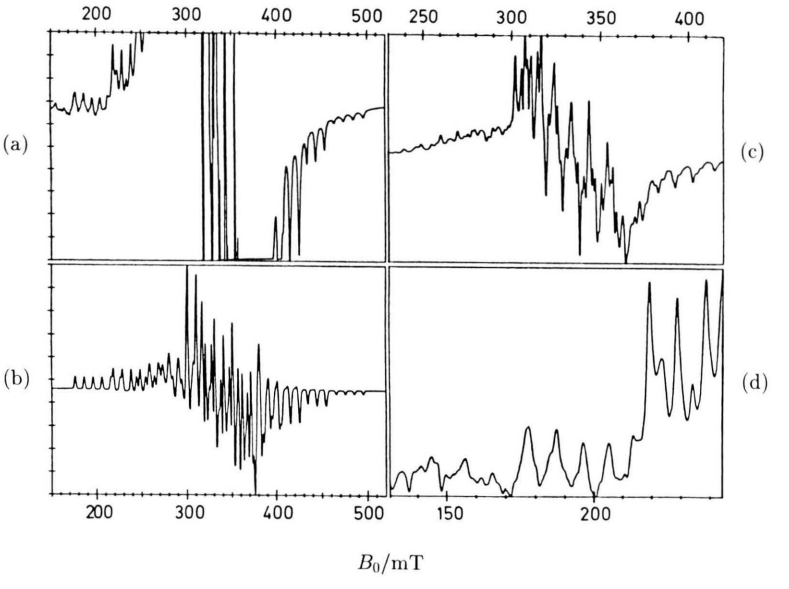

Fig. 1. K–Cd langbeinite. Diagram of peak positions of the Mn^{2+} EPR spectrum (single crystal, X band) as dependent on temperature T, indicating a phase transition around 410 K.

Fig. 2. K–Ca langbeinite, $P2_12_12_1$ phase. Powder spectrum of Mn^{2+} at room temperature (X-band, 9.389 GHz). Left, overview: (a) Experimental, (b) simulation. Right, details: (c) Central region with reduced amplification, (d) low field region with enhanced amplification.

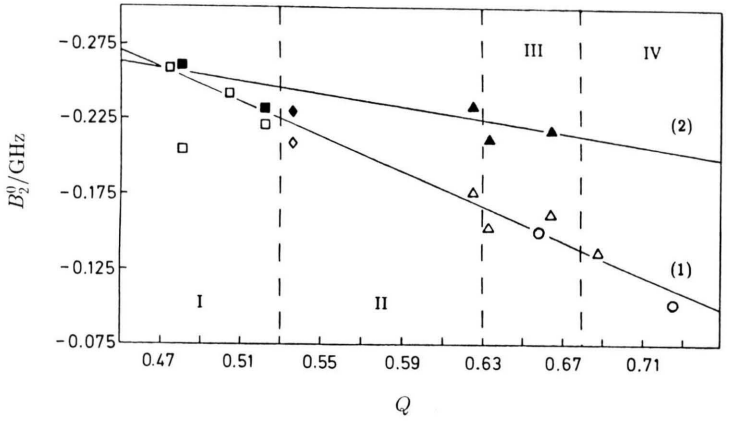

Fig. 3. ZFS parameter B_0^2 of Mn^{2+} centers in the cubic (high temperature) phase of some langbeinites vs. ratio of cationic radii, $Q = r_B/r_A$ (data from [23]). Open symbols: Center (1), full symbols: Center (2). Regression lines are plotted for both centers. The symbols refer to the divalent B cation: □ Mg, ◇ Zn, △ Cd, ○ Ca. For the Q regions I ··· IV see text.

The assumption of only one distinct defect center is sufficient in all cases except for K–Zn langbeinite. The sign of B_0^2 is estimated from the ratio of HFS parameters A_z of the low and high field sextet [43] (A_z(low)/A_z(high) in Table 2), presupposing a negative sign of hyperfine splitting constants A_i [23]. For the samples which are known to exist in the orthorhombic $P2_12_12_1$ phase (Table 1), the ZFS parameters are found to be positive. Therefore langbeinites with negative B_2^m are likely to represent one of the low temperature phases other than $P2_12_12_1$. A negative sign of B_2^0 is also found for the cubic phase $P2_13$ [23], which points to a relatively close structural similarity of $P2_13$ and the phase in question. Such a similarity to $P2_13$ is known for the monoclinic ($P2_1$) as well as the triclinic (P1) phase [16]. We have tentatively assumed that the phase in question be the monoclinic $P2_1$ one, which is not inconsistent with the Hikita classification scheme [17].

This assignment, together with other examples where the phase subsequent to the cubic one if any is well characterized, suggests a rough classification with respect to transition temperatures: The transition $P2_13 \rightarrow P2_1$ is observed for cases where $T_P \lesssim 190$ K (first class of the Hikita scheme [17]), while $P2_13 \rightarrow P2_12_12_1$ is found for $T_P \gtrsim 190$ K (second Hikita class).

To summarize, the EPR parameters of Mn^{2+} centers in the low temperature phases of langbeinites are in accordance with an irregularly distorted octahedral coordination by 6 oxygens. This is either elongated along the magnetic z-axis ($B_2^m < 0$, assumed phase $P2_1$) or compressed and, on the average, more distorted ($B_2^m > 0$, phase $P2_12_12_1$).

Temperature Dependence of EPR Parameters

The temperature dependence of EPR parameters may reflect different effects which cannot be resolved without information from other methods [44]. These may be (i) implicit effects, i.e. the temperature dependence of the crystal volume, (ii) explicit effects, i.e. an influence of temperature on the EPR parameters due to a coupling of the $3d^5$ ground state with excited $3d^44s^1$ states [45, 46] as mediated by lattice vibrations [46, 47], and (iii) other, e.g. precursory, effects. Since, moreover, experimental uncertainties will not allow in any case for an assessment, we summarize the temperature dependence of ZFS parameter B_2^0, HFS parameter A_z and linewidth ΔH_{PP} in an only qualitative manner.

In the high temperature phase, $|B_2^0|$ depends little on temperature T. There is a best a slight decrease with decreasing T (except for Rb–Mg langbeinite). In the low temperature phases (monoclinic as well as orthorhombic), on the other hand, $|B_2^0|$ is sometimes found to decrease remarkably with increasing temperature (e.g. K–Ca, Rb–Ca, NH_4–Cd, K–Cd langbeinite, Fig. 1), changing in non-linear manner when approaching T_P. This may be considered a hint at a precursory effect in the low temperature phase. The degree of that variation is seemingly not correlated with the phase transition temperature.

The HFS parameters are, in most cases, independent of temperature within experimental uncertainty; a discontinuous change is found on the transition from the cubic to the orthorhombic phase. However, for the high temperature (cubic) phase of some examples (Rb–Mg, Tl–Mg, Rb–Ca, Rb–Cd and Tl–Cd langbeinite) the experimental uncertainty is small enough to reveal a significant increase of the mean values A with decreasing temperature. This is rather unexpected since the decrease of crystal volume, as an implicite effect, would result in an opposite tendency [48, 49]. Thus this finding is probably related to explicite effects.

Linewidths ΔH_{PP} could be determined with sufficient accuracy only for the high temperature phase. If no phase transition takes place, ΔH_{PP} increases in approximately linear manner on decreasing temperature. On the other hand, in case that a phase transition occurs, ΔH_{PP} is not only generally larger but is the more increased the closer T approaches the EPR detectable transition temperature T_P. One may speculate as to whether that curvature results from passing over unnoticed phase transitions, since for the respective langbeinite (Cd–Tl) transitions are reported to occur between about 110 ··· 130 K (Table 1). However, a correspondingly curved $\Delta H_{PP} - T$ dependence is found e.g. with NH_4–Cd langbeinite for which there is only one phase transition known. Therefore that behaviour provides evidence of a precursory effect, possibly caused by a "softening" of the lattice which allows for an increasing variety of defect centers and thus for an increasingly broader distribution of ZFS parameters.

Discussion

Static and Dynamic Effects

Effects which influence the phase transition merely via crystallographic fine structure are termed "static" ones, in contrast to "dynamic" effects which relate to the temperature dependence of lattice parameters. It should be reminded that a relaxed region of the crystal is probed by EPR, the limiting relaxation state being determined by the size of the Mn^{2+} ion.

There is no significant correlation between the ZFS parameters of low temperature phases and the langbeinite composition. For the high temperature (cubic) phase, on the other hand, a systematic variation of the ZFS parameter B_0^2 with the ratio of cationic radii, $Q = r_B/r_A$ has been found [23]. This shall be reconsidered since there seems to be a certain correlation with the phase transition characteristics. In Fig. 3 the plot of B_2^0 for the cubic phase vs. Q is reproduced; the two centers found in that phase are marked (1), (2). Moreover four Q regions (I) to (IV) are tentatively distinguished.

(I) The region ($Q \leq 0.53$) corresponds to great distortions; here the Mg containing langbeinites are found which do not show a phase transition (down to ≈ 50 K).

(II) In that region of medium distortion, comprising K–Zn and Rb–Cd langbeinite, there is at least one EPR detectable phase transition below room temperature.

(III) This region ($0.63 < Q \leq 0.68$) corresponds to fairly small distortions. The respective langbeinites again show at least one phase transition below room temperature, the quality of their low temperature spectra, however, is much better than in region (II).

(IV) With still smaller distortions ($Q > 0.68$) there ocurs one EPR detectable phase transition above room temperature.

That rough correlation between distortion of Mn^{2+} centers and the very occurence of phase transitions may be understood as a static effect.

In Fig. 3, the open symbols (1) denote the more spacious of the two Mn^{2+} sites, which is preferably occupied [23]. One may cautiously conclude that it is particularly that site which is related in some manner to the occurence of phase transitions. Such an inference is in accord with results by Speer and Salje who also noticed a better correlation between phase transition and structural distortion parameters of just that site [2].

Dynamic effects in the above mentioned sense have not been noticed.

Description of Phase Transition

The EPR results indicate how the environment of the Mn^{2+} probe ion, which represents a B^{2+} site of the unrelaxed langbeinite lattice, is altered on decreasing temperature. Approaching the transition from the cubic $P2_13$ phase to any lower symmetric one, these alterations can be pictured in accordance with inferences from other methods as follows. The difference of the areas of both axial faces of the trigonally distorted oxygen octahedron around B^{2+} increases, and B^{2+} is shifted towards the larger face (cf. structure refinements [2]). That displacement results in decreasing differences of the B^{2+}–O bond lengths (cf. structure refinements [5], UV spectroscopy [50]). Consequently the trigonal distortion at the B^{2+} site is reduced (cf. $B_2^0(T)$ parameter of EPR [25–29] and this work). At the same time the array of ligands becomes less rigid. This softening facilitates a distribution of locally different B^{2+} sites (cf. EPR [25–29], in particular the $\Delta H_{PP}(T)$ dependence mentioned above, Raman spectroscopy [51]). On the macroscopic scale this causes a decreasing modulus of elasticity [18, 52, 53]. A phase transition occurs if the energy vanishes which is required to shift the atoms to the sites they occupy in the subsequent phase. The phase transition is of first order ([13, 21, 25–29, 30, 31, 54], our $B_2^0(T)$ results), reversible and shows no hysteresis.

Trigger Mechanism

The EPR characteristics should allow for some inferences concerning the trigger mechanism of the phase transitions. It seems therefore worthwhile to briefly regard the phase transition models proposed in the literature.

The model of two non-equivalent sublattices [55] may be left out of consideration since EPR based conclusions are not all possible. The SO_4^{2-} libration model [21] can be ruled out on grounds of Raman spectroscopic data [51].

From structure refinements a statistical distribution of oxygens amongst two positions has been concluded. The SO_4^{2-} order/disorder model [6] relates the phase transition to a confinement of the oxygens to one of these positions. The model, however, appears

inappropriate since EPR measurements (as well as other methods) indicate first order phase transitions.

Dvořák [11, 12] suggested that the lower symmetry phase emerges from the higher symmetry one by addition of an irreducible representation of the latter. The phase transition should be triggered by phonons. According to that model, however, a more pronounced dynamic effect than observed (influencing EPR via the temperature dependence of lattice parameters) would have been expected.

The BLVP (bond length variation parameter) model [5] claims the trigger mechanism to be related to the differing B^{2+}–O bond lengths which probably become equal at the phase transition temperature. This is not inconsistent with the EPR results.

The model of octahedral distortion [2] regards a phase transition as governed by the difference of thermodynamic stability of the cationic sites in the cubic and in the respective lower symmetric phase. The distortion parameters of the two B^{2+} sites are correlated with the temperature of the first phase transition. This model is adequate to account for a broad variety of experimental observations and is also consistent with our EPR results, provided one makes a qualitative extension by taking into consideration a lattice "softening", as suggested by the remarkable temperature dependence of linewidths ΔH_{pp}. Thus phase transitions appear to be essentially triggered by thermodynamic differences of cationic sites, viz. static effects.

[1] G. Gattow and J. Zemann, Z. anorg. allg. Chem. **293,** 233 (1958).
[2] D. Speer and E. Salje, Phys. Chem. Minerals **13,** 17 (1986).
[3] M. Kahrizi and M. O. Steinitz, Solid State Commun. **66,** 375 (1988).
[4] A. Zemann and J. Zemann, Acta Cryst. **10,** 409 (1957).
[5] M. J. L. Percival, W. W. Schmahl and E. Salje, Phys. Chem. Minerals **16,** 569 (1989).
[6] N. Yamada, M. Maeda and H. Adachi. J. Phys. Soc. Japan **50,** 907 (1981).
[7] Hok Nam Ng and C. Calvo, Can. J. Chem. **53,** 1449 (1975).
[8] B. Březina and M. Glogarová, phys. stat. sol. (a) **11,** K39 (1972).
[9] T. Hikita, T. Kudo, Y. Chubachi and T. Ikeda, J. Phys. Soc. Japan **41,** 349 (1976).
[10] T. Hikita, Y. Chubachi and T. Ikeda, J. Phys. Soc. Japan **44,** 525 (1978).
[11] V. Dvořák, phys. stat. sol. (b) **52,** 93 (1972).
[12] V. Dvořák, phys. stat. sol. (b) **66,** K87 (1974).
[13] S. C. Abrahams, F. Lissalde and J. L. Bernstein, J. Chem. Phys. **68,** 1926 (1978).
[14] H. Oelkrug, T. Brückel, D. Hohlwein, A. Hoser and W. Prandl, Phys. Chem. Minerals **16,** 246 (1988).
[15] S. C. Abrahams and J. L. Bernstein, J. Chem. Phys. **67,** 2146 (1977).
[16] N. Yamada and S. Kawano, J. Phys. Soc. Japan **43,** 1016 (1977).
[17] T. Hikita, M. Kitabatake and T. Ikeda, J. Phys. Soc. Japan **49,** 1421 (1980).
[18] T. Ikeda and G. Yasuda, Japan J. Appl. Phys. **14,** 1287 (1975).
[19] M. Maeda, J. Phys. Soc. Japan **49,** 1090 (1980).
[20] N. Yamadi, J. Phys. Soc. Japan **46,** 561 (1979).
[21] F. Lissalde, S. C. Abrahams, J. L. Bernstein and K. Nassau, J. Appl. Phys. **50,** 845 (1979).
[22] Y. Ishibashi and Y. Takagi, Japan J. Appl. Phys. **15,** 1621 (1976).
[23] T. Böttjer, G. Lehmann and M. Stockhausen, Z. Naturforsch. **47a,** 849 (1992).
[24] T. Böttjer and M. Stockhausen, Z. Naturforsch. **47a,** 1257 (1992).
[25] I. Tatsuzaki, J. Phys. Soc. Japan **17,** 1312 (1962).
[26] S. K. Misra and S. Z. Korczak, J. Phys. **C19,** 4353 (1986).
[27] D. Suresh Babu, G. S. Sastry, M. D. Sastry, and A. G. I. Dalvi, J. Phys. **C17,** 4245 (1984).
[28] S. K. Misra and S. Z. Korczak, J. Phys. **C20,** 4485 (1987).
[29] S. K. Misra and S. Z. Korczak, Solid State Commun. **61,** 665 (1987).
[30] B. Březina and A. Fouskova, Kristall und Technik **13,** 623 (1978).
[31] V. Devarajan and E. Salje, J. Phys. **C17,** 5525 (1984).
[32] S. Kreske and V. Devarajan, J. Phys. **C15,** 7333 (1982).
[33] T. Hikita, H. Sekiguchi and T. Ikeda, J. Phys. Soc. Japan **43,** 1327 (1977).
[34] J. Boerio-Goates, J. T. Artman and B. F. Woodfield, Phys. Chem. Minerals **17,** 173 (1990).
[35] T. Hikita, S. Sato, H. Sekiguchi and T. Ikeda, J. Phys. Soc. Japan **42,** 1656 (1977).
[36] F. Jona and R. Pepinsky, Phys. Rev. **103,** 1126 (1956).
[37] H. Ohshima and E. Nakamura, J. Phys. Chem. Solids **27,** 481 (1966).
[38] M. Glogarová and J. Fousek, phys. stat. sol. (a) **15,** 579 (1973).
[39] C. F. Buhrer and L. Ho, Appl. Optics **3,** 314 (1964).
[40] V. N. Moiseenko, V. G. Pozdeev and V. I. Pastukhov, Sov. Phys. Solid State **25,** 1262 (1983).
[41] A. M. Antonenko, M. D. Volnyanskii and V. G. Pozdeev, Sov. Phys. Solid State **25,** 1065 (1983).
[42] B. T. Deshmukh, S. V. Bodade and S. V. Moharil, phys. stat. sol. (a) **98,** 239 (1986).
[43] A. Abragam and B. Bleaney, Electron Paramagnetic Resonance of Transition Ions. Clarendon Press, Oxford, 1970.
[44] W. M. Walsh Jr., J. Jeener and N. Bloembergen, Phys. Rev. **139,** A1338 (1965).
[45] T. Gregorkiewicz and S. W. Biernacki, J. Phys. **C13,** 1285 (1980).
[46] E. Šimánek and R. Orbach, Phys. Rev. **145,** 191 (1966).
[47] K. Zdansky, phys. stat. sol. (a) **28,** 181 (1968).
[48] G. Lehmann, J. Phys. Chem. Solids **41,** 919 (1980).
[49] W. M. Walsh Jr., Phys. Rev. **122,** 762 (1961).
[50] M. J. L. Percival and E. Salje, Phys. Chem. Minerals **16,** 563 (1989).
[51] V. Devarajan and E. Salje, Phys. Chem. Minerals **13,** 25 (1986).
[52] M. Glogarová, phys. stat. sol. (a) **22,** K69 (1974).
[53] M. Maeda, J. Phys. Soc. Japan **47,** 1581 (1979).
[54] Y. Yamada, Y. Chubachi and T. Ikeda, J. Phys. Soc. Japan **45,** 1638 (1978).
[55] V. Dvořák and Y. Ishibashi, J. Phys. Soc. Japan **41,** 548 (1976).